

Determination of the Structure and Geometry of N-Heterocyclic Carbenes on Au(111) using High-Resolution Spectroscopy

Giacomo Lovat,^a Evan A. Doud,^b Deyu Lu,^c Gregor Kladnik,^{de} Michael S. Inkpen,^a Michael L. Steigerwald,^b Dean Cvetko,^{def} Mark S. Hybertsen,^c Alberto Morgante,^{*dg} Xavier Roy,^{*b} Latha Venkataraman,^{*ab}

N-heterocyclic carbenes (NHCs) bind very strongly to transition metals due to their unique electronic structure featuring a divalent carbon atom with a lone pair in a highly directional sp^2 -hybridized orbital. As such, they can be assembled into monolayers on metal surfaces that have enhanced stability compared to their thiol-based counterparts. The utility of NHCs to form such robust self-assembled monolayers (SAMs) was only recently recognized and many fundamental questions remain. Here we investigate the structure and geometry of a series of NHCs on Au(111) using high-resolution x-ray photoelectron spectroscopy and density functional theory calculations. We find that the N-substituents on the NHC ring strongly affect the molecule–metal interaction and steer the orientation of molecules in the surface layer. In contrast to previous reports, our experimental and theoretical results provide unequivocal evidence that NHCs with N-methyl substituents bind to undercoordinated adatoms to form flat-lying complexes. In these SAMs, the donor-acceptor interaction between the NHC lone pair and the undercoordinated Au adatom is primarily responsible for the strong bonding of the molecules to the surface. NHCs with bulkier N-substituents prevent the formation of such complexes by forcing the molecules into an upright orientation. Our work provides unique insights into the bonding and geometry of NHC monolayers; more generally, it charts a clear path to manipulating the interaction between NHCs and metal surfaces using traditional coordination chemistry synthetic strategies.

Introduction

N-heterocyclic carbenes (NHCs) are exceptionally strong σ -donor ligands capable of binding to virtually any transition metal. They are receiving increasing interest for their ability to form functional self-assembled monolayers (SAMs) on metal surfaces.^{1–8} Johnson, Crudden and their respective coworkers have demonstrated that NHC-based SAMs exhibit remarkable thermal and chemical stability that go well beyond thiol-based

SAMs on Au,^{1, 7} opening the door to novel applications in selective heterogeneous catalysis,^{9, 10} nanotechnology¹¹ and sensing.² Moreover, the strength and directionality of NHC–metal bonds, by now well-established in coordination chemistry, offer exciting new possibilities for passivating and/or manipulating the work function of metal surfaces.¹² While a substantial body of work has been devoted to NHCs since their discovery,^{13–21} this research has thus far mainly focused on the design of homogeneous catalysts. By contrast, many fundamental questions regarding the structure of NHC SAMs and their electronic coupling with metal surfaces remain unanswered.^{1, 7, 8, 22} Recently, some unique insights have been provided through the application of NHCs as linker groups in molecular-scale electronics.^{23, 24}

To date, most models of NHC-bound SAMs on metal surfaces postulate that the molecules adopt an upright geometry, with the heterocyclic system perpendicular to the surface.^{7, 8, 22, 25–28} In this orientation, a donor-acceptor interaction from the carbene lone pair to a surface atom is the primary contribution to the NHC–metal bond. In contrast, Baddeley, Papageorgiou, and their respective co-workers recently reported that some NHCs can form flat-lying mononuclear complexes (NHC)₂M (M = Cu, Ag, Au) on surfaces, where the coordinated metal site is pulled out of the surface

^a Department of Applied Physics and Applied Mathematics, Columbia University, New York, New York 10027, United States

^b Department of Chemistry, Columbia University, New York, New York 10027, United States

^c Center for Functional Nanomaterials, Brookhaven National Laboratory, Upton, New York

^d CNR-IOM Laboratorio Nazionale TASC, Basovizza SS-14, km 163.5, 34012 Trieste, Italy

^e Faculty of Mathematics and Physics, University of Ljubljana, Jadranska 19, Ljubljana, Slovenia

^f J. Stefan Institute, Jamova 39, SI-1000, Ljubljana, Slovenia

^g Department of Physics, University of Trieste, via A. Valerio 2, 34127, Trieste, Italy.

Electronic Supplementary Information (ESI) available: Synthetic details for the NHC precursors. Additional details regarding the preparation of the samples, high-resolution XPS measurements, NEXAFS measurements, theoretical calculations, as well as any additional experimental and theoretical data. See DOI: 10.1039/x0xx00000x

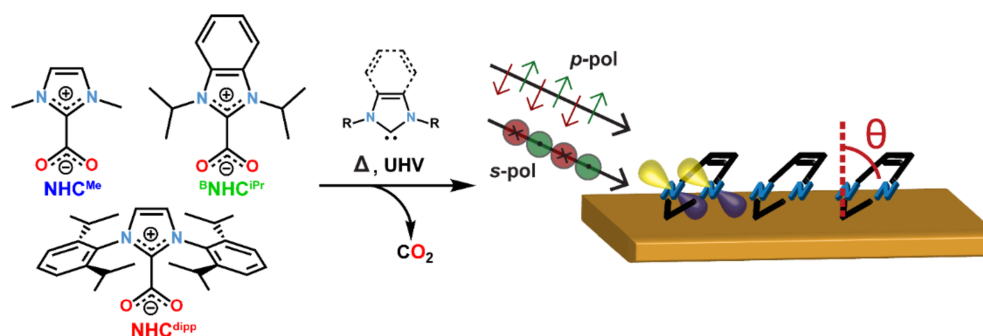


Fig. 1 Schematic showing the molecular structure of the NHC precursors, the thermal decomposition/sublimation deposition approach to create the NHC monolayers, and the NEXAFS dichroism measurement. Free NHC molecules are generated in the gas phase upon heating

plane.^{23, 29} Such adatoms are key structural components in SAMs of thiol molecules on Au(111),³⁰ and provide a clear experimental signature of surface reorganization induced by strong molecule-surface interactions. With the exception of a single report utilizing high resolution electron energy loss spectroscopy (HREELS),²³ the conflicting conclusions regarding the structure of NHC SAMs may be attributed to the use of scanning tunneling microscope (STM) imaging or low resolution x-ray photoelectron spectroscopy (LR-XPS) to probe these systems.²⁴ Such methods do not provide the chemical sensitivity required to determine the precise orientation of NHCs in SAMs, the nature of their bonding to the surface, nor the unambiguous detection of any associated Au adatoms. As a result, the role of N-substituents in influencing NHC SAM structure remains ill-defined.

In this work, we use synchrotron radiation to perform high-resolution x-ray photoelectron spectroscopy (HR-XPS) and near-edge x-ray absorption fine-structure spectroscopy (NEXAFS), and combine these measurements with density functional theory (DFT) calculations to establish a detailed picture of the geometry and bonding of a series of NHCs assembled on Au(111) in ultra-high vacuum (UHV). HR-XPS is highly sensitive to the chemical composition of the NHC layer and detects small changes to core-level electron binding energies that result from NHC–Au interactions, providing unique measurements of surface coverage and surface adatom density. NEXAFS allows us to unequivocally determine the orientation of the molecules relative to the surface by probing their unoccupied electronic states. Such information is key to understanding the relationship between the NHC molecular structure and their adsorption geometry, and can only be obtained through spectroscopic measurements as surface imaging techniques only focus on small areas and cannot resolve precisely the orientation of molecules bound to the surface. By rationalizing our experimental results using DFT calculations, we quantify the impact of the NHC structure and conformation on the strength of the molecule–Au interaction. Importantly, we show that through changes in the substituents on the N atoms, we can alter the steric environment around the carbenic C atom, which strongly affects the surface tilt angle and adsorption behavior of the molecules. This study complements and extends previous important efforts to characterize these systems, and also shows how thermal annealing in combination with careful selection of

N-substituents can modulate the structure of NHCs on Au(111) surfaces.

Results and discussion

Three NHCs with different steric properties are investigated: 1,3-dimethylimidazol-2-ylidene (NHC^{Me}), 1,3-diisopropylbenzimidazol-2-ylidene (NHC^{iPr}), and 1,3-bis(2,6-diisopropylphenyl)imidazol-2-ylidene (NHC^{dipp}). Details for the syntheses of the NHC precursors are found in the Electronic Supplementary Information (ESI). Monolayers were prepared in UHV via thermal decomposition/sublimation of NHC–CO₂ precursors,²² as illustrated in Figure 1 and described in the SI. Briefly, the precursors are placed in a Pyrex cell and connected to the pre-chamber through a leak valve. This cell is evacuated, heated to ~70 °C, and the carbene is introduced as a vapor into a pre-chamber containing a clean Au(111) crystal kept between -20 and -30 °C for ~5 min while maintaining a partial molecular pressure of 10⁻⁷ mbar. After deposition we confirm that the molecules deposited on the substrate have lost their CO₂ moieties, ostensibly through thermal decomposition, by measuring the O 1s spectrum of the layer using XPS.²²

To determine the orientation of the NHC relative to the Au (111) surface normal (defined as the tilt angle θ in Figure 1), we first present NEXAFS dichroism results for each molecule.³¹ Figure 2a shows the NEXAFS spectra collected at the N K-edge with the electric field of the incident photons perpendicular (*p*-polarization) and parallel (*s*-polarization) to the surface for NHC^{Me}, NHC^{iPr}, NHC^{dipp} monolayers. The key result is that the dichroism (which is evidenced by the differences in the NEXAFS spectra using *s*- and *p*-polarized photons) vary with the carbene N-substituents.³¹ The lowest energy NEXAFS resonance at ~401 eV, arising from the N 1s → π^* -LUMO (lowest unoccupied molecular orbital) transition, is strongly enhanced with *p*-polarized photons for NHC^{Me}, moderately enhanced for NHC^{iPr}, and virtually absent for NHC^{dipp}; the opposite trend is observed for *s*-polarized photons. Since the π^* -LUMO is delocalized over the whole imidazole ring for all three molecules, we can use the relative intensities of the ~401 eV NEXAFS *p*-polarized and *s*-polarized peaks to determine the average tilt angle θ for each carbene monolayer.³¹ We find that NHC^{Me} is almost flat ($\theta \sim 72^\circ$), NHC^{iPr} has an intermediate tilt angle ($\theta \sim 40^\circ$), and NHC^{dipp} is almost standing up ($\theta \sim 13^\circ$). The small tilt angle for NHC^{dipp} can

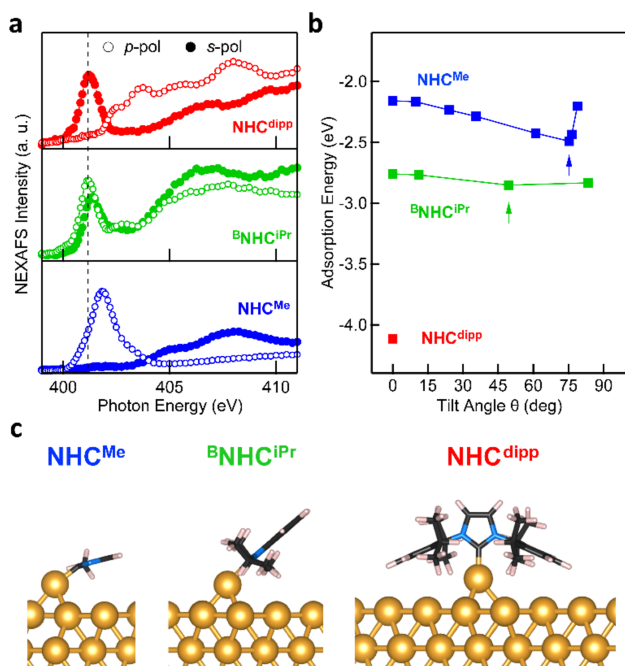


Fig. 2 (a) NEXAFS spectra collected at the N K-edge for NHC^{Me} (blue, bottom panel), ^BNHC^{iPr} (green), and NHC^{dipp} (red) monolayers on Au(111). Each spectrum is measured using x-ray photons with incident electric field in a plane perpendicular to the surface (*p*-pol, empty circles) or in a plane parallel to the surface (*s*-pol, filled circles). The N 1s \rightarrow π^* -LUMO resonance (\sim 401 eV, dashed black line) is significantly enhanced in *p*-pol for NHC^{Me}, and in *s*-pol for NHC^{dipp}, indicating a tilt angle $\theta \sim 72^\circ$ and $\sim 13^\circ$ respectively. For ^BNHC^{iPr}, both *s*- and *p*-pol spectra show the π^* -LUMO resonance, yielding $\theta \sim 40^\circ$. (b) Calculated adsorption energy of NHC^{Me} (blue) and ^BNHC^{iPr} (green) on an Au adatom as a function of θ . The adsorption energy of NHC^{dipp} (red) is calculated only for $\theta = 0^\circ$. The arrows indicate the lowest energy structure tilt angles, in good agreement with experimental observations. (c) DFT-optimized energy minimum structure of a single NHC^{Me}, ^BNHC^{iPr} and NHC^{dipp} adsorbed on an Au adatom sitting on a hollow site of an Au(111) slab. These structures are consistent with the experimentally observed tilt angles.

be attributed to the steric bulk introduced by the side groups forcing the molecule to stand and preventing the NHC-ring from interacting directly with the surface. This is corroborated by the NHC^{dipp} NEXAFS spectra collected at the C K-edge (Figure S1).

It is remarkable that these variations in the tilt angle do not result in significant differences in the NHC monolayer stability as a function of temperature. Indeed, XPS measurements show that NHC^{Me}, ^BNHC^{iPr} and NHC^{dipp} all come off the surface around $\sim 300^\circ\text{C}$ (either through desorption or decomposition) (Figure S2). This implies that all three NHCs have, despite their varied orientations, form strong donor-acceptor bonds to Au, as van der Waals interactions alone are unlikely to result in high desorption temperatures for such small cyclic compounds.³² The nature of the NHC–Au bond in these monolayers, and/or their macroscopic structure, is likely more complex than readily determined from the NEXAFS data alone. We therefore turn to DFT calculations to provide further insights.

Two adsorption models are explored using DFT calculations: in these models, the NHC molecule is adsorbed either on a pristine Au(111) surface or an Au adatom sitting on a hollow site of the Au(111) surface. Total energy and geometry optimization calculations, detailed in the ESI, are performed using Quantum Espresso³³ with an exchange and correlation functional that

accounts for van der Waals interactions^{34, 35} and a 4-layer Au(111) slab comprising 3 \times 3, 4 \times 3, and 5 \times 5 surface unit cells for NHC^{Me}, ^BNHC^{iPr} and NHC^{dipp}, respectively. The adsorption energy is defined as the difference between the energy of the combined system and the sum of the energies for each component separately, and is negative for bound systems. The adsorption energy of NHC^{Me} in a constrained flat-lying geometry on an Au(111) slab is small (-0.91 eV), as the carbene lone pair lies parallel to the Au slab and does not form a strong σ -bond to an Au atom (Figure S3). Removing the constraint on the tilt angle in this model results in NHC^{Me} adopting a binding geometry nearly normal to the Au(111) surface ($\theta \sim 15^\circ$); this geometrical change is accompanied by a 0.58 eV increase of the adsorption energy of the molecule (-1.49 eV; Figure S4). These results, however, are at odds with the NEXAFS data indicating that $\theta \sim 72^\circ$ for NHC^{Me}.

A significantly different outcome is obtained when the NHCs are relaxed on top of an Au adatom, as shown in Figure 2b. The adsorption energy for the NHCs at different tilt angles is calculated by constraining the geometry of the NHC ring relative to the surface normal. In its most stable conformation (Figure 2b,c), NHC^{Me} has a tilt angle $\theta \sim 75^\circ$, in excellent agreement with the NEXAFS data, and an adsorption energy of -2.49 eV, which is 1 eV larger than when NHC^{Me} is bound to a flat Au(111) surface. The maximum adsorption energy for ^BNHC^{iPr} is -2.85 eV, corresponding to an optimized tilt angle $\theta \sim 50^\circ$. The adsorption energy for ^BNHC^{iPr}, however, is only weakly dependent on θ , a consequence of the competition between steric repulsion imparted by the bulkier side substituents and the van der Waals interaction of the benzene ring towards the Au surface. The weak dichroism in the NEXAFS spectrum of ^BNHC^{iPr} (Figure 2a) agrees well with the theoretical results: the shallow energy minimum implies that there is no strong driving force to orient the molecule in a preferential geometry. Moreover, the computed lowest energy θ for ^BNHC^{iPr} is close to the theoretical angle at which no dichroism is expected ($\theta \sim 55^\circ$). Due to its bulkier N-substituents, NHC^{dipp} can only bind vertically, irrespective of the presence of an adatom (Figure S5). The adsorption energies for NHC^{dipp} bound to the Au(111) surface and to an Au adatom are -2.69 eV and -4.11 eV, respectively.

For all three NHCs, the adsorption energy is larger when the molecule binds to an Au adatom. This is the result of the metal *s*- and *d*-orbitals being more accessible in the adatom, which leads to a stronger donor-acceptor bond as reflected in the shorter NHC–Au bond length when the molecule is modeled on an Au adatom (see Table S1). Among the three NHCs, however, NHC^{dipp} stands out: the calculated adsorption energy for the adatom-bound model is significantly larger than the corresponding values for the other two NHCs. We attribute this difference to the van der Waals interactions of the dipp groups with the Au surface. The difference in adsorption energy between the pristine surface-bound and adatom-bound models is also significantly larger for the NHC^{dipp} system than for the

other two NHCs. This can be explained by steric effects between the bulky dipp substituents and the surface, which significantly lengthen the NHC–Au bond (2.15 Å) and distort the molecule when NHC^{dipp} is bound to a pristine Au(111) surface. By contrast, when NHC^{dipp} is bound to an Au adatom, the dipp groups are further away from the surface, the carbenic C atom can get closer to the Au adatom (NHC–Au^{ad} bond length = 2.02 Å), and the molecule can relax to a less strained conformation. This is most easily seen looking at the orientation of the dipp groups, which are almost parallel to the surface in the perfect slab model (Figure S5) and close to the unstrained geometry in the adatom model (i.e. the C^{NHC}–N^{NHC}–C^{dipp} angle is ~124°; Figure 2c).

The DFT calculations presented above suggest that NHCs bind significantly more strongly to an Au adatom than to a perfect Au(111) surface; XPS measurements can detect the presence of such adatoms on the surface. Figure 3a presents the N 1s core level XPS spectra of NHC^{Me}, ^BNHC^{iPr} and NHC^{dipp} monolayers. A single N 1s peak is observed in the NHC^{Me} and NHC^{dipp} spectra, consistent with only one type of N-containing species on the surface. The spectrum of ^BNHC^{iPr} shows two peaks: the first and more intense main peak is very close in energy to that of NHC^{dipp} and is attributed to surface-bound ^BNHC^{iPr}; the second, lower-energy peak is attributed to incipient second-layer growth and/or a small amount of undissociated ^BNHC^{iPr}–CO₂ adducts on the surface. Note that the NHC^{Me} N 1s peak (401.2 eV) is at a significantly higher binding energy than the corresponding peaks for the ^BNHC^{iPr} and NHC^{dipp} monolayers (~400.5 eV). The correlation between this shift and the positions of the NEXAFS N 1s → π*-LUMO resonance (Figure 2a) for these monolayers indicates that the latter is related to the N 1s core binding energy (an initial state effect). Such a shift to higher binding energy results from charge depletion at the N in NHC^{Me} monolayer as its π-electron system interacts with the Au surface. This is consistent with the orientation of the molecule determined by NEXAFS.

Figure 3b compares the XPS spectra of the Au core level 4f spin-orbit doublet for a clean Au(111) surface and an NHC^{Me} monolayer grown on the same Au(111) surface.³⁶ The NHC^{Me} monolayer spectrum features a doublet of satellite peaks at higher binding energies; fits of the Au 4f_{7/2} peak indicate that the new set of peaks is shifted by +1.1 eV with respect to the Au bulk component (Figure S6a). Two contributions can explain the difference in the binding energy of the Au 4f peak: a chemical shift and a screening shift that both result for an Au atom that is significantly lifted from the surface. Comparing the area under each peak, we find that 1/6 of the surface is covered by adatoms (Figure S6a).

To explore the origin of these satellite peaks, we consider two possible adsorption scenarios for NHC^{Me}: (1) the adsorption of a single NHC^{Me} on an Au adatom (NHC^{Me}–Au^{ad}), and (2) the formation of a flat-lying bis(NHC) complex with an Au adatom (NHC^{Me}–Au^{ad}–NHC^{Me}). We calculate the binding energy shift for the Au adatom 4f core level relative to the bulk (ΔE_{BE}) using the transition state model^{37, 38} of the excited system and the projector augmented-wave method implemented in the Vienna *Ab initio* Simulation Package (VASP).^{39, 40} Figure 3c presents the

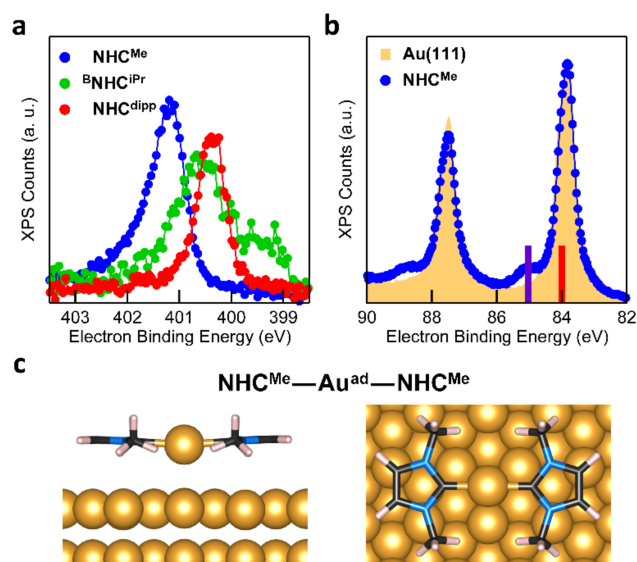


Fig. 3 (a) XPS N 1s spectra of NHC^{Me} (blue), ^BNHC^{iPr} (green), and NHC^{dipp} (red) monolayers on Au(111). The NHC^{Me} N 1s peak is shifted to higher binding energy relative to both NHC^{dipp} and ^BNHC^{iPr}. (b) XPS Au 4f_{5/2, 7/2} spectra of a clean Au(111) surface (yellow filled area) and the NHC^{Me} monolayer (blue) on the same Au(111) surface. The satellite peaks at ~1 eV higher binding energy are attributed to the presence of a high density of Au adatoms. Solid bars on the binding energy axis are the calculated XPS peak positions for bulk Au (red, 84.00 eV) and the Au adatom in the NHC^{Me}–Au^{ad}–NHC^{Me} complex (purple, 85.03 eV) adsorbed on the Au(111) slab. (c) DFT-optimized energy minimum structure of the NHC^{Me}–Au^{ad}–NHC^{Me} complex adsorbed on a 4-layer Au(111) slab (only the upper two layers are shown). The NHC^{Me} rings are nearly coplanar to the surface and the adatom is on a hollow site.

computed structure for the fully relaxed NHC^{Me}–Au^{ad}–NHC^{Me} complex adsorbed on a 5×4 unit cell. For the complex, $\Delta E_{BE} = 0.91$ eV, in good agreement with the experimental value ($\Delta E_{BE} = 1.1$ eV). By contrast, the computed binding energy shift for NHC^{Me}–Au^{ad} ($\Delta E_{BE} = 0.16$ eV) is much smaller, suggesting that the satellite peaks in Figure 3b come from NHC^{Me}–Au^{ad}–NHC^{Me} complexes on the surface. The formation of this bis(NHC) complex pulls the Au adatom away from the surface by more than 1 Å (Au^{ad}–Au^{surf} distance is 2.06 and 3.09 Å for NHC^{Me}–Au^{ad} and NHC^{Me}–Au^{ad}–NHC^{Me}, respectively). The change in the electron binding energy of the Au adatom, which is due to chemical shift and screening effects, is similar to what has been observed in thiol-based monolayers.³⁶

As a comparison, the Au 4f XPS spectrum of the NHC^{dipp} monolayer shows no satellite peaks at higher binding energy because the bulky dipp groups prevent the formation of such bis(NHC) complexes (Figure S6b). A careful analysis of the STM images presented in a recent study²² of NHC^{Me} monolayers on Au(111) further corroborate our conclusion that the molecules indeed form flat-lying NHC^{Me}–Au^{ad}–NHC^{Me} complexes as opposed to NHC^{Me}–Au^{ad} species oriented normal to the surface, as originally proposed. To illustrate this point, Figure S7 compares an STM image simulated from our optimized structure and an experimental STM image reproduced from Wang et al.²²

The behavior of ^BNHC^{iPr} differs from that of NHC^{Me} and NHC^{dipp}, and this suggests that the formation of the flat-lying bis(NHC) complexes is a thermally activated process. Figure 4a

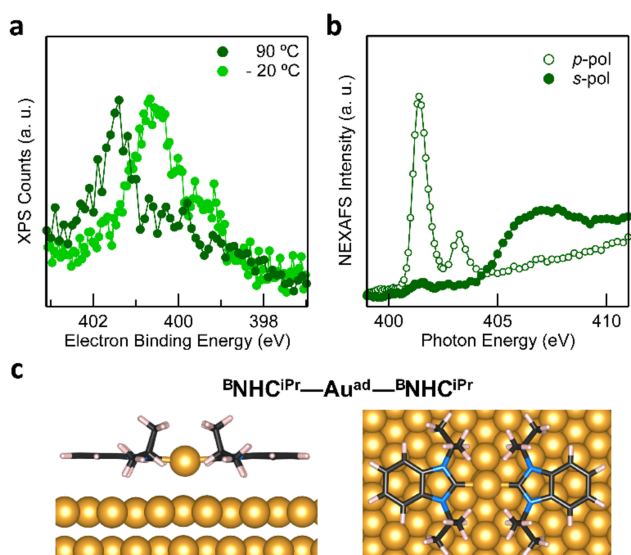


Fig. 4 (a) XPS N 1s spectra of a ${}^{\text{B}}\text{NHC}^{\text{iPr}}$ monolayer deposited on a cold substrate at $-20\text{ }^{\circ}\text{C}$ (light green), and then annealed to $90\text{ }^{\circ}\text{C}$ (dark green). The broad peak in the low-temperature spectrum comprises different components likely due to multiple molecular adsorption sites and/or of second-layer molecules. Thermal annealing generates a single sharp N 1s peak shifted to higher binding energy by $\sim 1\text{ eV}$. (b) NEXAFS spectrum collected at the N K-edge for the ${}^{\text{B}}\text{NHC}^{\text{iPr}}$ monolayer annealed to $90\text{ }^{\circ}\text{C}$: a strong dichroism is clearly visible. The $\text{N } 1s \rightarrow \pi^*\text{-LUMO}$ resonance is strongly enhanced in p -pol indicating that the molecules lie nearly flat on the surface. (c) DFT-optimized energy minimum structure of a ${}^{\text{B}}\text{NHC}^{\text{iPr}}\text{-Au}^{\text{ad}}\text{-}{}^{\text{B}}\text{NHC}^{\text{iPr}}$ complex adsorbed on an Au(111) 5×7 slab. Note that the adatom is above a hollow site on the Au(111) surface.

compares the N 1s XPS spectrum of a ${}^{\text{B}}\text{NHC}^{\text{iPr}}$ monolayer deposited at $-20\text{ }^{\circ}\text{C}$ with that of the monolayer annealed to $90\text{ }^{\circ}\text{C}$. The low-temperature monolayer shows a broad peak at $\sim 400.5\text{ eV}$, indicating the formation of a mostly disordered surface structure (Figure 2a). Remarkably, the XPS peak shape and energy change significantly upon thermal annealing. The high temperature N 1s XPS peak is sharp and shifted to a higher binding energy ($\sim 401.5\text{ eV}$), similar to that observed for the $\text{NHC}^{\text{Me}}\text{-Au}^{\text{ad}}\text{-NHC}^{\text{Me}}$ complexes (Figure 3a). The striking reorganization of the molecular layer is also captured in the NEXAFS dichroism collected at the N K-edge (Figure 4b): the $\text{N } 1s \rightarrow \pi^*\text{-LUMO}$ resonance is greatly enhanced in p -polarized light, pointing to a nearly flat geometry for the annealed monolayer.

These spectroscopic changes make the adsorption behavior of ${}^{\text{B}}\text{NHC}^{\text{iPr}}$ at high temperature similar to that of NHC^{Me} , and prompted us to investigate theoretically the possibility that ${}^{\text{B}}\text{NHC}^{\text{iPr}}$ forms flat-lying bis(NHC) complexes, provided sufficient energy is available. Similar to its NHC^{Me} analogue, the modeled structure of the ${}^{\text{B}}\text{NHC}^{\text{iPr}}\text{-Au}^{\text{ad}}\text{-}{}^{\text{B}}\text{NHC}^{\text{iPr}}$ complex on an Au(111) slab (Figure 4c) shows that the Au adatom is pulled away from the surface by $\sim 1\text{ \AA}$ (Table S1). While this should in principle also alter the Au 4f XPS spectra, we do not observe Au satellite peaks in Figure S6b. The lower surface density of ${}^{\text{B}}\text{NHC}^{\text{iPr}}$ accounts for this result: using the intensity of the N 1s XPS peak, we estimate that the ${}^{\text{B}}\text{NHC}^{\text{iPr}}$ surface density at $90\text{ }^{\circ}\text{C}$ is ~ 10 times lower than that of NHC^{Me} at $-20\text{ }^{\circ}\text{C}$, and thus too small to detect Au adatoms. Two effects combine to explain the lower surface density: the footprint of the flat-lying benzannulated ${}^{\text{B}}\text{NHC}^{\text{iPr}}$ is

larger than that of NHC^{Me} , and the elevated temperature for the measurement leads to a further decrease in the packing density.

Conclusions

The strong carbene–Au interaction offers exciting opportunities as an alternative to the traditional thiol–Au bond, which suffers from limited chemical, electrochemical and thermal stability. By combining high-resolution x-ray photoelectron spectroscopy and computational modeling, this work reveals how adsorption energy, molecular orientation and metal surface structure are closely interconnected in a series of NHC monolayers. We find that NHCs bind significantly more strongly to an Au adatom than to a flat Au(111) surface, and show that with sufficient time and thermal energy, the molecule is capable of reorganizing the underlying gold surface structure. The orientation of the NHC on the surface is determined by the N-substituents: the smallest group – methyl – favors a planar geometry in which the NHC ring is parallel to the surface and organized into $\text{NHC}^{\text{Me}}\text{-Au}^{\text{ad}}\text{-NHC}^{\text{Me}}$ complexes. Bulkier groups force the molecule into a more vertical orientation and prevent the formation of such flat-lying complexes. By thermally annealing the monolayer, we show it is possible to modulate the structure of surface-bound NHCs by converting them from adatom bound orientations to bis(NHC) complexes, as shown for ${}^{\text{B}}\text{NHC}^{\text{iPr}}$. While the initial orientation of NHCs on the surface appears to have little effect on the high thermal stability of NHCs SAMs, we expect that the geometry and electronic structure of the surface-bound carbenes will ultimately prove critical in controlling their (electro)chemical stability, reactivity and functionality, through steric hindrance of reactive sites as well as the extent of intermolecular and molecule-surface interactions.

Conflicts of interest

There are no conflicts to declare

Acknowledgements

We thank Albano Cossaro for assisting with the experiments. The experimental and theoretical work was supported primarily by the Center for Precision Assembly of Superstratic and Superatomic Solids at Columbia University, an NSF MRSEC (award number DMR-1420634) and by NSF CHE-1807654. E.A.D and X.R. thank the Donors of the American Chemical Society Petroleum Research Fund for support (ACS PRF# 57062-DNI10). X.R. also acknowledges the Air Force Office of Scientific Research under AFOSR Award No. FA9550-18-1-0020. M.S.I. was supported by a Marie Skłodowska Curie Global Fellowship (MOLCLICK: 657247) within the Horizon 2020 Programme. D.C. and G.K. acknowledge partial financial support from the Slovenian Research Agency (program No. P1-0112). G.K. acknowledges financial support from the SIR grant SUNDYN [Nr. RBSI14G7TL, CUP B82I15000910001] of the Italian Ministry of Education, Universities and Research MIUR. Our research used resources of Center for Functional Nano-materials, which is a

U.S. DOE Office of Science Facility, and the Scientific Data and Computing Center, a component of the Computational Science Initiative, at Brookhaven National Laboratory, under Contract No. DE-SC0012704.

Notes and References

1. C. M. Crudden, J. H. Horton, I. I. Ebralidze, O. V. Zenkina, A. B. McLean, B. Drevniok, Z. She, H.-B. Kraatz, N. J. Mosey, T. Seki, E. C. Keske, J. D. Leake, A. Rousina-Webb and G. Wu, *Nat. Chem.*, 2014, 1-6.
2. C. M. Crudden, J. H. Horton, M. R. Narouz, Z. Li, C. A. Smith, K. Munro, C. J. Baddeley, C. R. Larrea, B. Drevniok, B. Thanabalasingam, A. B. McLean, O. V. Zenkina, I. I. Ebralidze, Z. She, H.-B. Kraatz, N. J. Mosey, L. N. Saunders and A. Yagi, *Nat. Commun.*, 2016, 7.
3. X. Ling, S. Roland and M. P. Pileni, *Chemistry of Materials*, 2015, **27**, 414-423.
4. X. Ling, N. Schaeffer, S. Roland and M. P. Pileni, *Langmuir*, 2015, **31**, 12873-12882.
5. M. J. MacLeod and J. A. Johnson, *J. Am. Chem. Soc.*, 2015, **137**, 7974-7977.
6. S. Roland, X. Ling and M. P. Pileni, *Langmuir*, 2016, **32**, 7683-+.
7. A. V. Zhukhovitskiy, M. G. Mavros, T. Van Voorhis and J. A. Johnson, *J. Am. Chem. Soc.*, 2013, **135**, 7418-7421.
8. T. Weidner, J. E. Baio, A. Mundstock, C. Grosse, S. Karthaus, C. Bruhn and U. Siemeling, *Australian Journal of Chemistry*, 2011, **64**, 1177-1179.
9. J. A. Mata, M. Poyatos and E. Peris, *Coord. Chem. Rev.*, 2007, **251**, 841-859.
10. K. V. S. Ranganath, S. Onitsuka, A. K. Kumar and J. Inanaga, *Catalysis Science & Technology*, 2013, **3**, 2161-2181.
11. R. W. Y. Man, C. H. Li, M. W. A. MacLean, O. V. Zenkina, M. T. Zamora, L. N. Saunders, A. Rousina-Webb, M. Narnbo and C. M. Crudden, *J. Am. Chem. Soc.*, 2018, **140**, 1576-1579.
12. H. K. Kim, A. S. Hyla, P. Winget, H. Li, C. M. Wyss, A. J. Jordan, F. A. Larrain, J. P. Sadighi, C. Fuentes-Hernandez, B. Kippelen, J.-L. Brédas, S. Barlow and S. R. Marder, *Chemistry of Materials*, 2017, **29**, 3403-3411.
13. A. J. Arduengo, R. L. Harlow and M. Kline, *J. Am. Chem. Soc.*, 1991, **113**, 361-363.
14. S. Diez-Gonzalez, N. Marion and S. P. Nolan, *Chem. Rev.*, 2009, **109**, 3612-3676.
15. D. Enders, O. Niemeier and A. Henseler, *Chem. Rev.*, 2007, **107**, 5606-5655.
16. W. A. Herrmann, *Angew. Chem. Int. Ed.*, 2002, **41**, 1290-1309.
17. W. A. Herrmann, M. Elison, J. Fischer, C. Kocher and G. R. J. Artus, *Angew. Chem. Int. Ed.*, 1995, **34**, 2371-2374.
18. W. A. Herrmann, M. Elison, J. Fischer, C. Kocher and G. R. J. Artus, *Chem. Eur. J.*, 1996, **2**, 772-780.
19. W. A. Herrmann and C. Kocher, *Angew. Chem. Int. Ed.*, 1997, **36**, 2162-2187.
20. N. Marion, S. Diez-Gonzalez and S. P. Nolan, *Angew. Chem. Int. Ed.*, 2007, **46**, 2988-3000.
21. N. Marion and S. P. Nolan, *Chem. Soc. Rev.*, 2008, **37**, 1776-1782.
22. G. Wang, A. Ruhling, S. Amirjalayer, M. Knor, J. B. Ernst, C. Richter, H. J. Gao, A. Timmer, H. Y. Gao, N. L. Doltsinis, F. Glorius and H. Fuchs, *Nat. Chem.*, 2017, **9**, 152-156.
23. C. R. Larrea, C. J. Baddeley, M. R. Narouz, N. J. Mosey, J. H. Horton and C. M. Crudden, *ChemPhysChem*, 2017.
24. A. Bakker, A. Timmer, E. Kolodzeiski, M. Freitag, H. Y. Gao, H. Moenig, S. Amirjalayer, F. Glorius and H. Fuchs, *J. Am. Chem. Soc.*, 2018.
25. E. C. Hurst, K. Wilson, I. J. S. Fairlamb and V. Chechik, *New Journal of Chemistry*, 2009, **33**, 1837-1840.
26. C. Richter, K. Schaepe, F. Glorius and B. J. Ravoo, *Chemical Communications*, 2014, **50**, 3204-3207.
27. Q. Tang and D. E. Jiang, *Chemistry of Materials*, 2017, **29**, 6908-6915.
28. A. V. Zhukhovitskiy, M. J. MacLeod and J. A. Johnson, *Chem. Rev.*, 2015, **115**, 11503-11532.
29. L. Jiang, B. Zhang, G. Medard, A. P. Seitsonen, F. Haag, F. Allegretti, J. Reichert, B. Kuster, J. V. Barth and A. C. Papageorgiou, *Chem. Sci.*, 2017, **8**, 8301.
30. A. Cossaro, R. Mazzarello, R. Rousseau, L. Casalis, A. Verdini, A. Kohlmeyer, L. Floreano, S. Scandolo, A. Morgante, M. L. Klein and G. Scoles, *Science*, 2008, **321**, 943-946.
31. J. Stohr, *NEXAFS Spectroscopy*, Heidelberg, 1992.
32. S. M. Wetterer, D. J. Lavrich, T. Cummings, S. L. Bernasek and G. Scoles, *J. Phys. Chem. B*, 1998, **102**, 9266-9275.
33. P. Giannozzi, S. Baroni, N. Bonini, M. Calandra, R. Car, C. Cavazzoni, D. Ceresoli, G. L. Chiarotti, M. Cococcioni and I. Dabo, *J. Phys.:Cond. Mat.*, 2009, **21**, 395502.
34. K. Berland, V. R. Cooper, K. Lee, E. Schröder, T. Thonhauser, P. Hyldgaard and B. I. Lundqvist, *Reports on Progress in Physics*, 2015, **78**, 066501.
35. D. C. Langreth, B. I. Lundqvist, S. D. Chakarova-Kack, V. R. Cooper, M. Dion, P. Hyldgaard, A. Kelkkanen, J. Kleis, L. Z. Kong, S. Li, P. G. Moses, E. Murray, A. Puzder, H. Rydberg, E. Schroder and T. Thonhauser, *J. Phys.:Cond. Mat.*, 2009, **21**.
36. A. Cossaro, L. Floreano, A. Verdini, L. Casalis and A. Morgante, *Phys. Rev. Lett.*, 2009, **103**.
37. C. Goransson, W. Olovsson and I. A. Abrikosov, *Phys. Rev. B*, 2005, **72**.
38. J. F. Janak, *Phys. Rev. B*, 1978, **18**, 7165-7168.
39. G. Kresse and J. Furthmuller, *Phys. Rev. B*, 1996, **54**, 11169.
40. G. Kresse and J. Furthmuller, *Computational Materials Science*, 1996, **6**, 15-50.